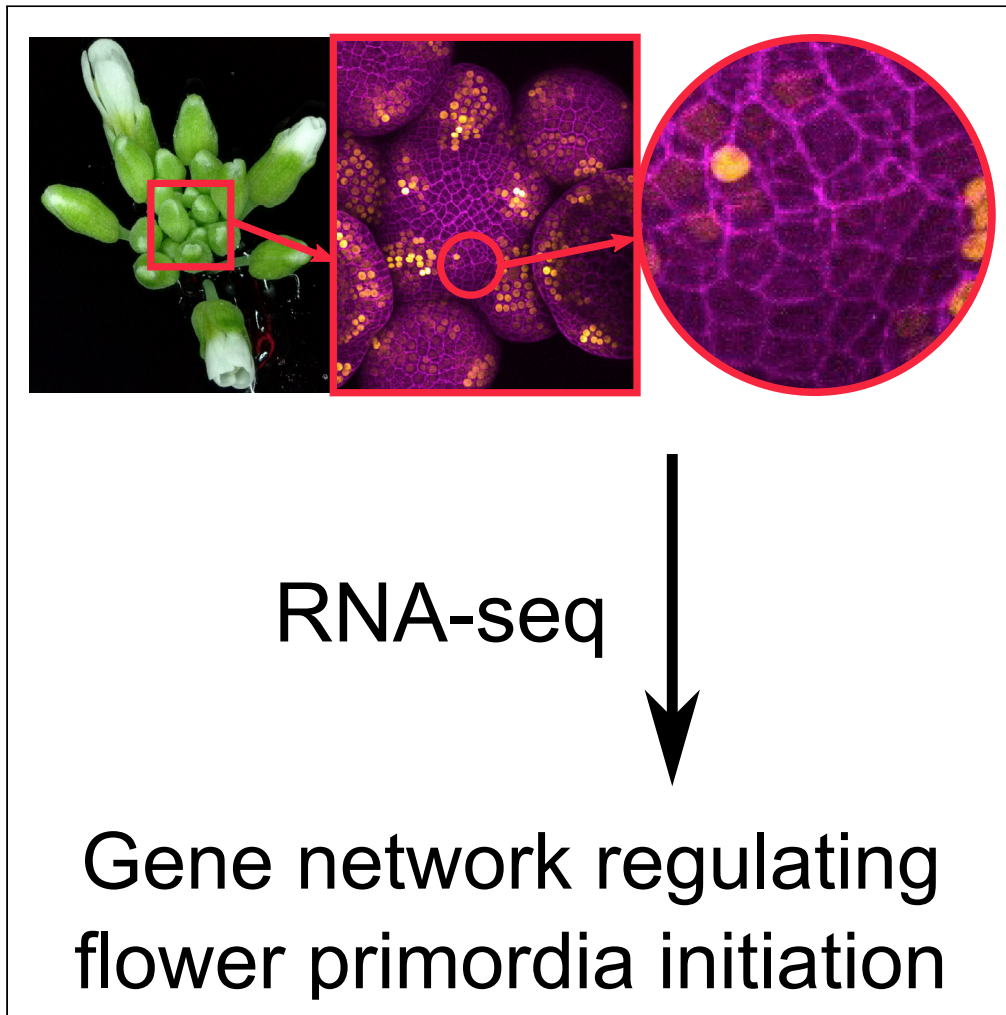


## Article

## Transcriptional reprogramming during floral fate acquisition



Antoine Larrieu,  
Géraldine  
Brunoud, Aurore  
Guérault, ..., Ykä  
Helariutta,  
François Parcy,  
Teva Vernoux

a.p.larrieu@leeds.ac.uk (A.L.)  
teva.vernoux@ens-lyon.fr (T.V.)

**Highlights**

Pharmacological  
approach to probe  
transcriptional responses  
in shoot meristems

Analysis of a shoot-  
specific network regulated  
by auxin during flower  
initiation

Two DOF transcription  
factors are induced in  
flower primordia

The DOF genes  
potentially link growth to  
organ identity acquisition

## Article

## Transcriptional reprogramming during floral fate acquisition

Antoine Larrieu,<sup>1,10,\*</sup> Géraldine Brunoud,<sup>1</sup> Aurore Guérault,<sup>1,11</sup> Stéphanie Lainé,<sup>1</sup> Lauriane Hennet,<sup>1</sup> Arnaud Stigliani,<sup>2,13</sup> Iris Gildea,<sup>3</sup> Jeremy Just,<sup>1</sup> Ludivine Soubigou-Taconnat,<sup>4,5</sup> Sandrine Balzergue,<sup>6,12</sup> Brendan Davies,<sup>7</sup> Enrico Scarpella,<sup>9</sup> Ykä Helariutta,<sup>3,8</sup> François Parcy,<sup>2</sup> and Teva Vernoux<sup>1,14,\*</sup>

## SUMMARY

**Coordinating growth and patterning is essential for eukaryote morphogenesis. In plants, auxin is a key regulator of morphogenesis implicated throughout development. Despite this central role, our understanding of how auxin coordinates cell fate and growth changes is still limited. Here, we addressed this question using a combination of genomic screens to delve into the transcriptional network induced by auxin at the earliest stage of flower development, prior to morphological changes. We identify a shoot-specific network suggesting that auxin initiates growth through an antagonistic regulation of growth-promoting and growth-repressive hormones, quasi-synchronously to floral fate specification. We further identify two DNA-binding One Zinc Finger (DOF) transcription factors acting in an auxin-dependent network that could interface growth and cell fate from the early stages of flower development onward.**

## INTRODUCTION

During morphogenesis of multicellular organisms, undifferentiated cells respond to endogenous cues and switch identity, resulting in the determination of cell fate patterns and in growth changes. How cell fate patterns and growth are synchronized to generate complex organisms with stereotypical organization is a key question in developmental biology. In plants, flowers are formed at the tip of shoot axes on the flanks of shoot apical meristems (SAMs), in a ring-shaped domain called the peripheral zone (PZ) (Denay et al., 2017). The small signaling molecule auxin, which is polarly transported, accumulates in few cells of the PZ where the activation of its transduction pathway leads to organogenesis (Reinhardt et al., 2003). In the model plant *Arabidopsis thaliana*, mutations affecting either polar auxin transport (e.g., *pin-formed 1* (*pin1*) or *pinoid* (*pid*)) or auxin signaling (e.g., *arf5/monopteros* (*mp*)) result in naked inflorescences where floral organogenesis fails (Bennett et al., 1995; Okada et al., 1991; Przemeck et al., 1996). Auxin primarily acts at the transcriptional level via two families of interacting transcription factors (TFs) and regulators, termed auxin response factors (ARFs) and auxin/indoleacetic acid (Aux/IAAs) (Vernoux et al., 2011). In response to auxin, ARF proteins reprogram gene expression, starting with genes with ARF binding sites, i.e. auxin response element (ARE), in their regulatory regions (Larrieu and Vernoux, 2015).

Despite the essential role of auxin during floral initiation and development, few genes have been identified as direct auxin targets in SAMs (Wu et al., 2015; Yamaguchi et al., 2013). These include the APETALA2 TFs *AINTEGUMENTA* (*ANT*) and *AINTEGUMENTA-LIKE 6/PLETHORA 3* (*AIL6/PLT3*), the plant-specific single copy TF *LEAFY* (*LFY*) and the YABBY TF *FILAMENTOUS FLOWER* (*FIL*). These TFs promote growth (*AIL6/ANT*), patterning (*FIL*, *LFY*), and floral identity acquisition (*LFY*), highlighting a dual function of auxin in regulating both growth and cell fate at the SAM. However, these genes are induced with a significant delay compared to the onset of auxin-induced transcription and are expressed only once the flower primordium starts growing out from the SAM (Caggiano et al., 2017; Heisler et al., 2005; Yamaguchi et al., 2013). Flower initiation occurs dynamically in only a small number of cells that cannot be easily isolated (Figure 1A) (Besnard et al., 2014), and this has so far prevented the analysis of the early network acting in the flower founder cells to initiate flower patterning and growth in response to auxin.

<sup>1</sup>Laboratoire Reproduction et Développement des Plantes, Univ Lyon, ENS de Lyon, CNRS, INRAE, 69342 Lyon, France

<sup>2</sup>Univ. Grenoble Alpes, CNRS, CEA, INRAE, BIG-LPCV, 38000 Grenoble, France

<sup>3</sup>Institute of Biotechnology, HiLIFE/Organismal and Evolutionary Biology Research Programme, Faculty of Biological and Environmental Sciences, and Viikki Plant Science Centre, University of Helsinki, 00014 Helsinki, Finland

<sup>4</sup>Institute of Plant Sciences Paris-Saclay (IP2S), CNRS, INRAE, Université Paris-Sud, Université d'Évry, Université Paris-Saclay, Bâtiment 630, Plateau de Moulon, 91192 Gif sur Yvette, France

<sup>5</sup>Institute of Plant Sciences Paris-Saclay (IP2S), CNRS, INRAE Université Paris-Diderot, Sorbonne Paris-Cité, Bâtiment 630, Plateau de Moulon, 91192 Gif sur Yvette, France

<sup>6</sup>IRHS-UMR1345, Université d'Angers, INRAE, Institut Agro, SFR 4207 QuaSaV, 49071 Beaucozéz, France

<sup>7</sup>Centre for Plant Sciences, School of Biology, Faculty of Biological Sciences, University of Leeds, Leeds, West Yorkshire LS2 9JT, UK

<sup>8</sup>The Sainsbury Laboratory, University of Cambridge, Cambridge CB2 1LR, UK

<sup>9</sup>Department of Biological Sciences, University of Alberta, CW-405 Biological Sciences Building, Edmonton, AB T6G 2E9, Canada

<sup>10</sup>Present address: Center for Plant Sciences, School of Biology, Faculty of Biological Sciences, University of Leeds, LS2 9JT UK

Continued



## RESULTS

### Genes and processes affected in mutant inflorescences deficient in auxin transport and signaling

To gain insight into the auxin-dependent network during flower initiation, we used complementary RNA-seq-based genomic analyses to obtain a global vision of the auxin-regulated gene network in the SAM before progressively converging on the identification of a high-confidence core network acting during the early phases of flower initiation (Figure 1B).

Initially, we profiled the transcriptome of dissected wild-type meristems (Col-0) and pin-shaped meristems of mutants *pin1-7*, *pid-9*, and *mp<sup>S319</sup>* (all loss-of-function alleles in Col-0 accession, *pin1-7* and Col-0 control already described in Armezzani et al., 2018). From these datasets, we identified 5483 differentially expressed (DE) genes (2927 up and 2556 down, Data S1) that were consistently DE in the three mutants (Figure 1C). In upregulated genes, the gene ontology (GO) “Response to cytokinins” (FDR =  $6.1 \times 10^{-8}$ ) was enriched, coherently with the primary function of cytokinin in stem cell niche specification (Figure 1D and Data S2). In downregulated genes, the GO term “Flower development” (FDR =  $1.7 \times 10^{-9}$ ) was enriched, showing that this approach effectively captured genes activated during floral organogenesis. However, the GO terms “Response to auxin” (FDR = 5.5E-2) and “Auxin-activated signaling pathway” (FDR = 1.5E-1) were only slightly overrepresented among the downregulated genes (Figure 1D, Data S2). This is likely because of secondary effects of the mutations, for instance compensatory physiological or mechanical changes of meristematic tissues due to long-term changes in auxin signaling activity and to the absence of flowers, hindering the identification of early auxin-responsive genes in SAMs.

### A model system to study auxin early responses in shoot meristems identifies a shoot-specific network

We thus designed an approach with an increased sensitivity to identify genes regulated by auxin during early organogenesis. We employed a pharmacological approach using the polar auxin transport inhibitor NPA to generate pin-like SAMs *in vitro* (termed NPA pins, Figures 2A–2D). These have been shown to generate a ring of organogenesis from cells in the periphery in response to exogenous auxin (Sassi et al., 2014). To further characterize cell identities in NPA pins and confirm their meristematic identity, we looked at the expression of the synthetic auxin reporter *pDR5-3xVENUS-N7* (Vernoux et al., 2011) and the endogenous reporters *pAHP6-GFP* (Besnard et al., 2014) and *pSTM-YFP-H4* (Verkest et al., 2005), which mark differentiated (*DR5* and *AHP6*) and undifferentiated (*STM*) cells of the PZ (Figures 2E–2H and S1A–S1I). We observed that while NPA pins have no or barely detectable *DR5* or *AHP6* expression, *STM* is expressed in most cells of the SAM periphery. These results indicate that while cells in the PZ of NPA pins have a meristematic identity, they remain in an undifferentiated state and unresponsive to auxin. Then, we looked at the effects of exogenous auxin treatments on the spatial and temporal dynamics of the three reporters using live imaging. While the *DR5* reporter accumulated high levels of fluorescence in all tissues except in the CZ, as expected, *AHP6* was induced only in the periphery (Figures 2I–2L and Videos S1 and S2). This expression pattern is strikingly similar to primordia-specific genes in *pin1* mutants (e.g. *LFY* and *ANT*) (Vernoux et al., 2000). In contrast, the *STM* reporter showed a progressive reduction of fluorescence over time in the periphery, consistent with its downregulation during primordia initiation (Figures S1J–S1M and Video S3) (Long et al., 1996). For the three markers, changes in fluorescence were detected after 60 min (Figure S1N). Together with previous reports (Sassi et al., 2014), our results establish an experimental framework and define a time window to analyze auxin responses during early stages of flower initiation in SAMs.

We thus profiled the transcriptome of NPA pins treated with or without auxin for 30 or 120 min to analyze the dynamics of early auxin responses. We identified 109 and 1448 induced as well as 39 and 1166 repressed genes after 30 and 120 min, respectively (Figures S2A and S2B, and Data S3). As the dynamics of *pDR5-3xVENUS* fluorescence accumulation in response to auxin in NPA pins is similar to what was previously reported in roots (Figure S2C, Videos S1 and S4) (Brunoud et al., 2012), we compared our “Shoot” auxin response transcriptome with a “Root” auxin response transcriptome generated using mature root tissues as the source of mRNA (De Rybel et al., 2012). We found that only 16% ( $n = 340$ ) of up- and 10% ( $n = 200$ ) of downregulated genes were common to both datasets (Figures 2M and S2D and Data S3). Incidentally, 41% ( $n = 851$ ) and 43% ( $n = 932$ ) of up- and 39% ( $n = 737$ ) and 51% ( $n = 1054$ ) of downregulated genes were either shoot or root-specific, respectively. Genes induced only in roots are mainly associated

<sup>11</sup>Present address: Department of Plant Molecular Biology, University of Lausanne, Biophore Building, 1015, Lausanne, Switzerland

<sup>12</sup>Present address: IRHS, Agrocampus-Ouest, INRA, Université d’Angers, 49071 Beaucaouzé, France

<sup>13</sup>Present address: The Bioinformatics Center, Department of Biology & Biotech Research and Innovation Center, University of Copenhagen, Ole Maaloes Vej 5, DK2200 Copenhagen N, Denmark

<sup>14</sup>Lead contact

\*Correspondence: a.p.larrieu@leeds.ac.uk (A.L.), teva.vernoux@ens-lyon.fr (T.V.)

<https://doi.org/10.1016/j.isci.2022.104683>

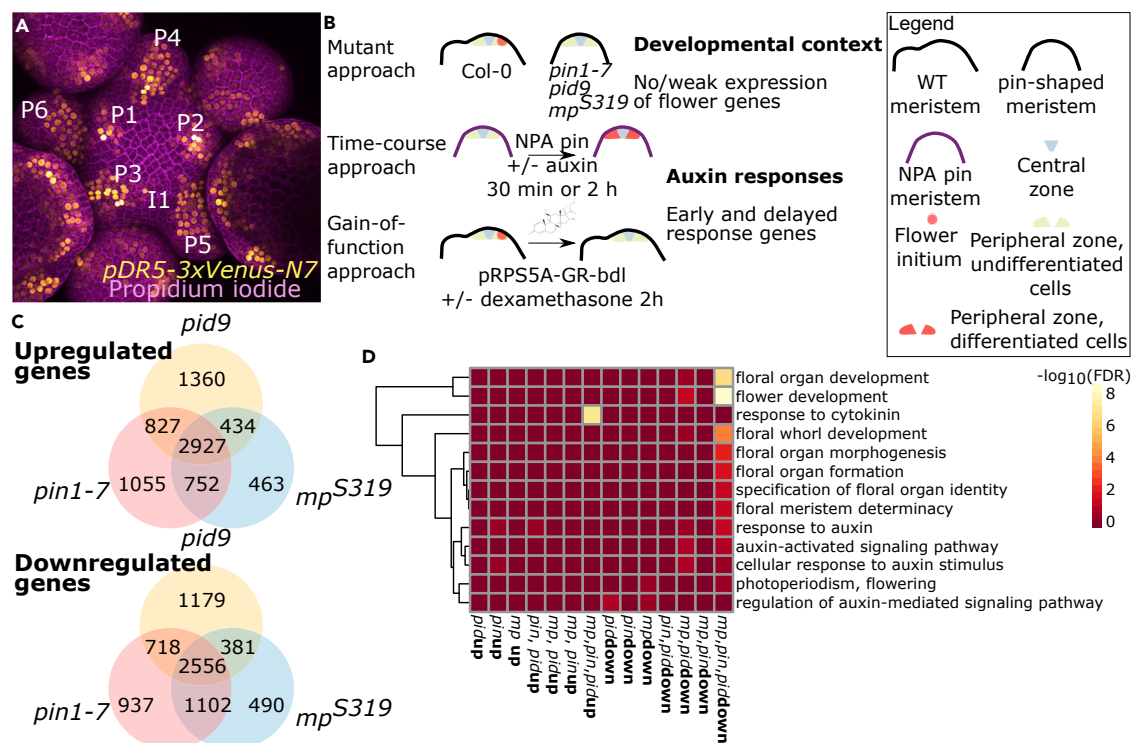


**Figure 1. Identification of auxin response genes during flower primordia establishment using a combination of RNA-seq screens**  
(A) *pDR5-3xVenus-N7* reporter in wild-type inflorescence SAM shows that auxin responses are activated before any morphological changes occur (I1 stage).  
(B) Three RNA-seq screen were used to identify auxin response genes during flower formation. These provide a developmental context, using flower-less mutants, and auxin responses, using two pharmacological approaches.  
(C) Venn diagram showing the overlap between the three mutant datasets.  
(D) Heatmap showing the  $-\log_{10}(\text{False Discovery Rate, FDR})$  for selected ontologies associated with auxin, cytokinin, and flower development in the mutant datasets.

with ribosome biogenesis, while repressed ones are involved in photosynthesis (Figure 2N and Data S4). In contrast, genes induced by auxin only in shoots are associated with lignin and wax biosynthesis, while repressed ones are involved in stress responses, primarily mediated by jasmonic acid (JA) (Figure 2N and Data S4). These results demonstrate the large differences in genomic auxin responses in shoots and roots. They indicate a strong differential competence between these tissues and identify a shoot-specific auxin-dependent network.

### A meta-analysis shows that resources are oriented toward growth during early flower primordia initiation

To further define a high-confidence auxin-dependent network acting during flower initiation, we consolidated our SAM auxin response transcriptome by also profiling the transcriptome of an inducible repressor of auxin signaling (*pRPS5A-GR-bdl* (Weijers et al., 2006), Figure 1B) using inflorescence tissues treated with or without  $10\mu\text{M}$  dexamethasone (dex) for 2 h. The short treatments allowed 121 downregulated and 40 upregulated genes to be identified (Figure S3A and Data S3). Since this is a gain-of-function approach, genes induced by auxin in NPA pins are expected to be downregulated with dex. Therefore, we discarded from further analyses genes showing incoherent fold changes ( $n = 6/161$ , Figure S3B). The overlap between dex and auxin datasets ( $n = 78/155$  (>50%), Figure S3B) demonstrates that both approaches are complementary and captured auxin-responsive genes. In addition, we found a significant enrichment in ARF5 *dap-seq* peak in the promoters of regulated genes compared to non-regulated genes ( $p\text{-val} = 2,9 \times 10^{-10}$ , hypergeometric test) (Figures S3D–S3I). For auxin-induced genes, this increase was most significant at 30 min, suggesting that our experiment captured early regulation of direct auxin targets. For further analyses, we separated early/direct targets (DE after 30 min of auxin treatments and/or after dex treatments) from delayed ones (DE only after 120 min of auxin treatments) (Figure S3C and Data S3).

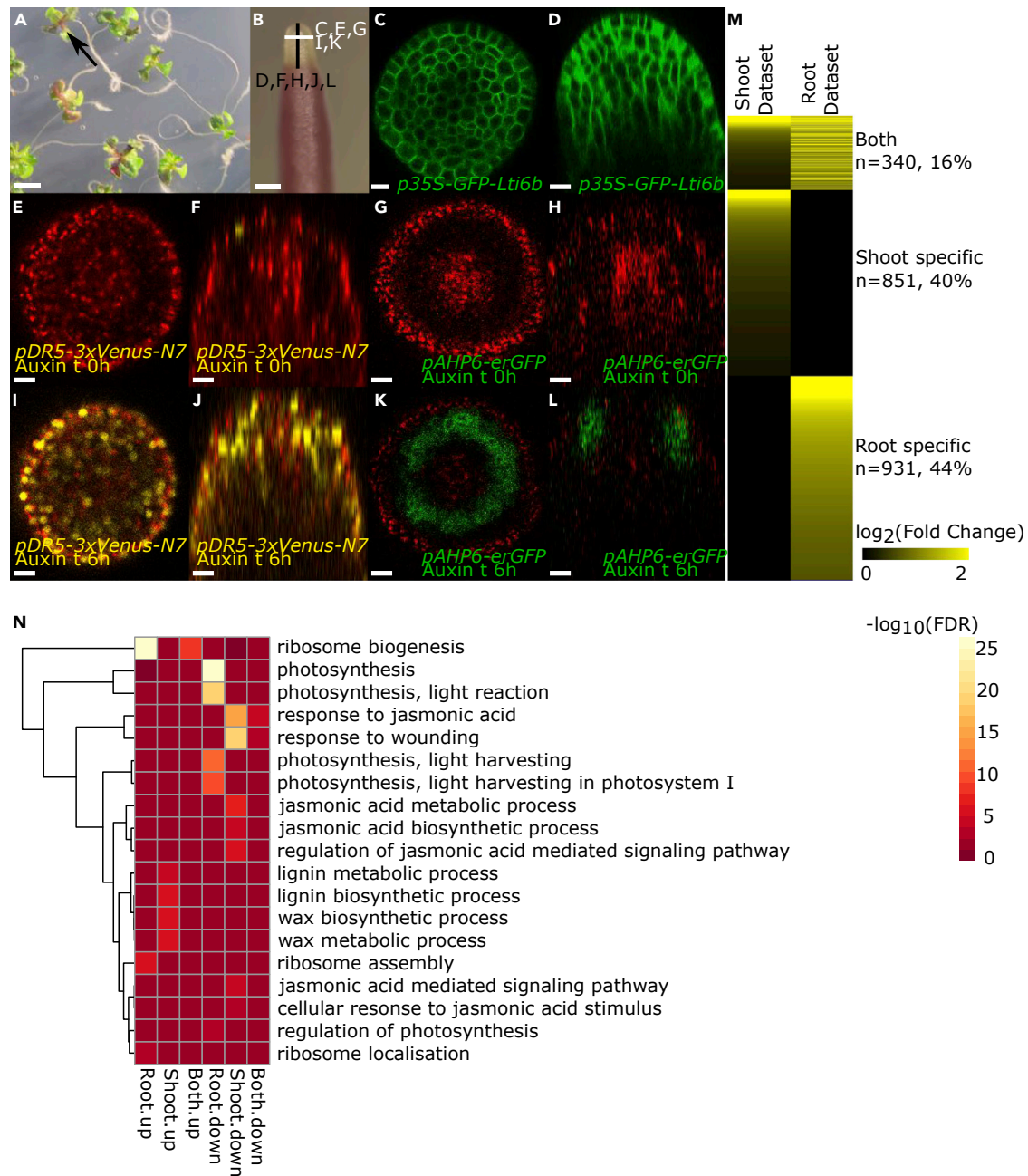


**Figure 2. NPA pin as a model system to study hormone responses in SAMs**  
 (A and B) Arabidopsis plants grown on Naphthylphthalamic acid (NPA, 10 $\mu$ M) produce naked inflorescences that morphologically resemble *pin* mutants. (C–L) Transverse (C,E,G,I,K) and longitudinal (D,F,H,J,L) sections, as represented by the white and black lines in B, of NPA pins expressing either a cell surface marker (*p35S-Lti6b-GFP*) (C and D), an auxin response marker (*pDR5-3xVenus-N7*) (E–F and I–J) or an AHP6 transcriptional reporter (*pAHP6-erGFP*) (G–H and K–L). NPA pins have been mock (C–H) or auxin (IAA, 1 $\mu$ M) treated (I–L) for 16 h. (M) Heat maps showing genes induced after 2 h of auxin treatments in roots (De Rybel et al., 2012) and/or in shoots (this study). (N) Selection of gene ontologies enriched either in the root, the shoot or in both datasets. Scale bar = 1mm (A), 60 $\mu$ m (B), 5 $\mu$ m (C–L).

We then cross-referenced the auxin response and dex datasets with the mutant datasets. We kept genes DE in at least two mutants and one pharmacological treatment, making sure that the signs of significant fold changes were consistent (Data S5). These filters led to 52 early and 289 delayed upregulated as well as 12 early and 370 delayed downregulated high-confidence genes (Figure 3A and Data S5). Ontologies enriched with the 52 early- and 284 late-induced genes include “Flower development” and “Response

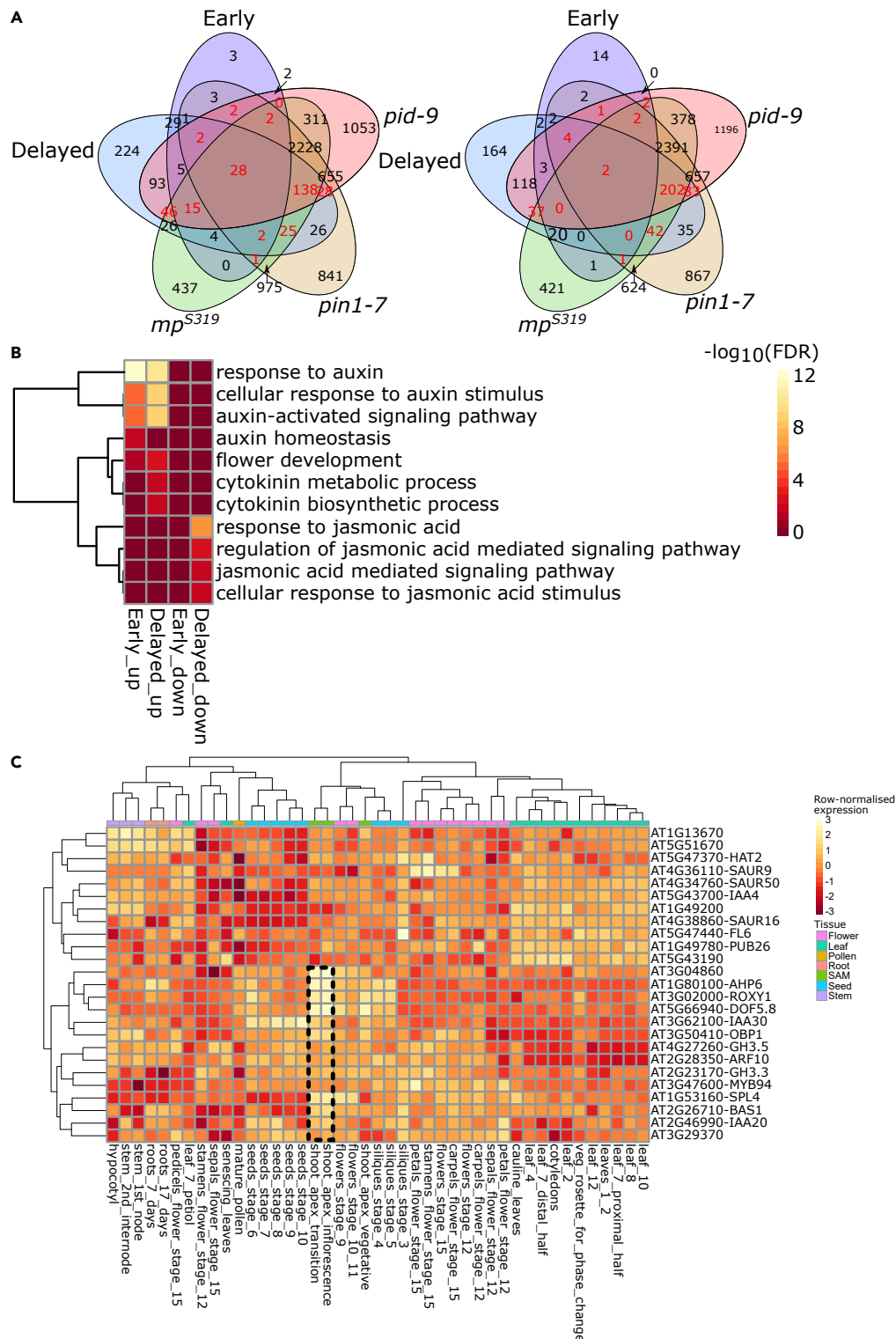


**Figure 3. Continued**

(B) Selection of gene ontologies enriched with early or delayed auxin-responsive genes (see text for definition).

(C) Hierarchical clustering of the 25 induced top targets (i.e. DEGs selected from the high-confidence list (criteria in Figure S3C)) but DE in all datasets (the mutants and all pharmacological treatments) across 43 different tissues highlights one cluster of genes with a shoot-specific expression patterns (dashed black square).

to auxin" while "Cytokinin metabolism" was only enriched with the delayed induced genes (Figure 3B and Data S6). While no ontologies were significantly enriched in early repressed genes, "Response to jasmonic acid" was again highly enriched in delayed repressed genes (Figure 3B and Data S6), and an enrichment was also found for "Response to salicylic acid" and "Response to abscisic acid". These results suggest that auxin induces first and almost immediately gene networks controlling cell fate in flower primordia. Cytokinins are essential for cell cycle activation and have recently been shown to be positive regulators of organ initiation at the SAM (Landrein et al., 2018). Conversely, jasmonic, salicylic, and abscisic acids repress growth during stress responses (Su et al., 2013; Yang et al., 2012). Auxin could thus prepare the growth phase through hormonal cross-talks and notably repression of stress hormones quasi-synchronously to cell fate specification. The flower master regulator LFY has also been shown to repress biotic stress responses (Winter et al., 2011). Our data indicate that orienting resources toward growth at the expense of stress responses could be a general auxin-dependent property of organogenesis at the shoot.

**DOF3.4/OBP1 and DOF5.8 are activated during primordia initiation and potentially link growth with floral fate acquisition**

To functionally assess the capacity of our approach to identify early regulators of organogenesis, we finally focused on a core network of 14 genes that are identified as consistently auxin-induced across all datasets and with preferential expression in inflorescence meristems (Figure 3C). Of these 14 genes, seven have been confirmed as expressed specifically at organ primordia initiation sites using *in situ* hybridization or reporter lines (IAA20 and IAA30 (Vernoux et al., 2011), AHP6 (Besnard et al., 2014), ROXY1 (Xing et al., 2005), MYB94 (Lee and Suh, 2015), SPL4 (Torti et al., 2012), and BAS1 (Bell et al., 2012)), one has a confirmed role during flower development (ARF10 (Liu et al., 2010)) and two others belong to the GH3 gene family, which regulates auxin metabolism (Staswick et al., 2002), and are markers associated with auxin-responsive tissues (Hagen et al., 1991) (Table S1). The remaining four genes encodes two proteins of unknown function and two DOF (DNA binding with one zinc finger) transcription factors (OBP1/DOF3.4 and DOF5.8). Using whole-mount *in situ* hybridization and translational reporters, we showed that both DOF genes are expressed and that the proteins accumulate at flower primordia initiation sites (Figures 4A–4D). OBP1 and DOF5.8 cluster together on a phylogenetic tree suggesting they might act redundantly (Figure S4 (Yanagisawa, 2002)), so we assessed their role using loss of function alleles and overexpressing lines. Although single and double mutants flowered earlier than the WT (Figure S5), they did not display conspicuous inflorescence phenotypes (Figure S6) or show defects in flower-expressed genes (Figure S7) suggesting both genes are dispensable under controlled growth conditions. However, when combined with the weak *mp*<sup>5319</sup> allele, we observed an aggravation of *mp* seedling phenotypes, notably the formation of tubular seedlings ("tubes"), a phenotype we never observed in single *mp*<sup>5319</sup> mutants (Figure 4E). These tubular seedlings are rootless and have an oval-shaped shoot structure missing cotyledons. This observation is compatible with both DOFs acting downstream of MP and show that they are required for organogenesis in *mp*<sup>5319</sup> background. Also, overexpression of OBP1 or DOF5.8 using the RPS5A promoter in wild type resulted in a delay in flowering (Figure S5), consistent with a regulatory role in flowering. Coherently, ontologies enriched with genes co-expressed either with OBP1 or DOF5.8 include "Flower Development" and "Shoot System Development" (Data S5). OBP1 has in addition been suggested to control the expression of cell cycle genes (Skirycz et al., 2008) and genes involved in cell growth and auxin responses are DE in a DOF5.8-inducible dominant-negative overexpression lines (Konishi and Yanagisawa, 2015). Overexpression of OBP1 or DOF5.8 under the RPS5A promoter induces defects in leaf morphology (Figure S6), consistent with a role on cell proliferation and growth. In addition, expression of DOF5.8, either WT or fused to a SUPRD repressor motif (Konishi and Yanagisawa, 2015), using an MP promoter leads to even more severe leaf phenotypes with smaller and highly serrated leaves (Figure S6). To test directly a role for OBP1 or DOF5.8 in proliferation, we induced expression of either OBP1 or DOF5.8 in the vascular tissue at the root tip, i.e. in cells where they are not normally expressed. This induction triggered extra cell proliferation leading to an increased number of vascular cell files (Figures 4F–4K), similarly to the effect observed with other DOF transcription factors involved in controlling radial growth in the root (Miyashima et al., 2019). Altogether, this suggests a scenario where these two DOF TFs could act downstream of auxin on flower development as regulators of growth, through a primary action on cell proliferation. Interestingly, the

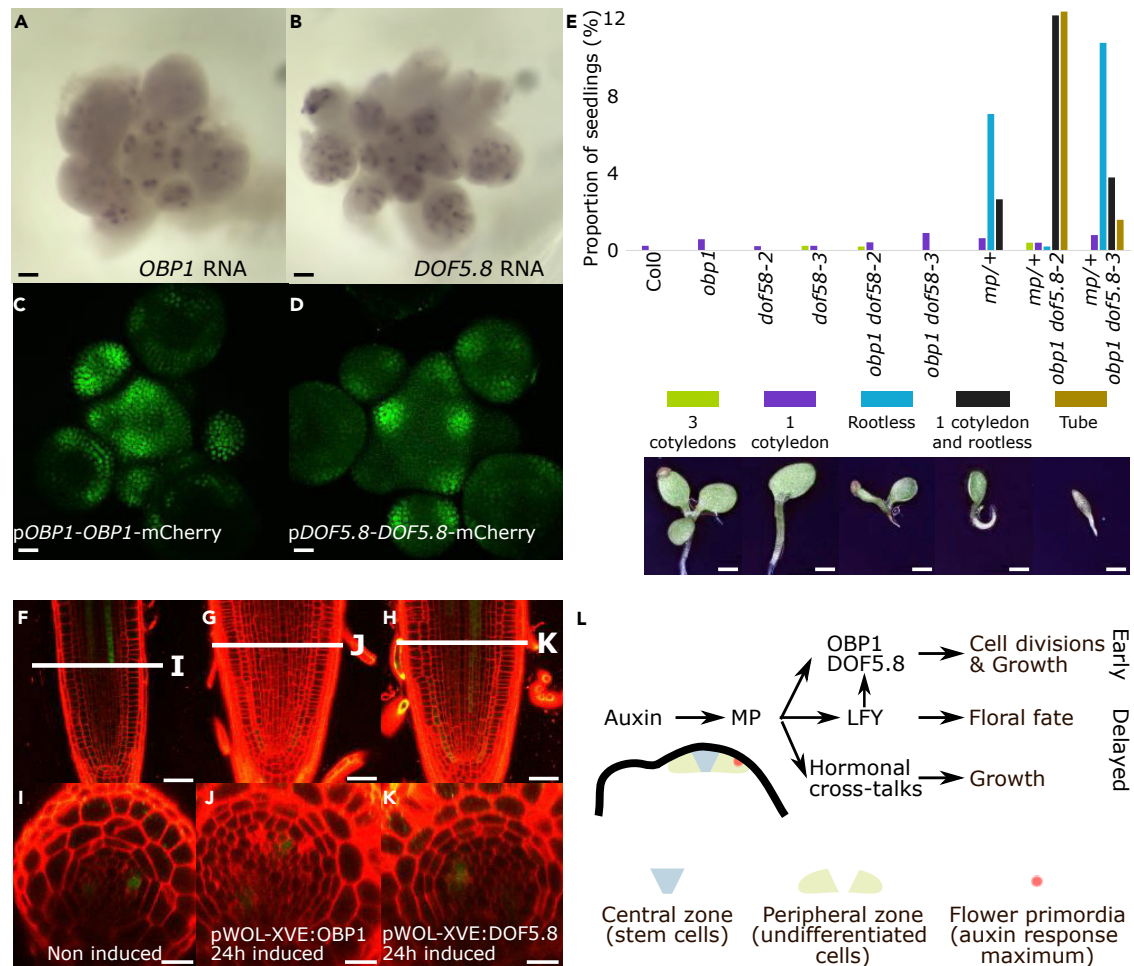


**Figure 4. OBP1 and DOF5.8 connect auxin and tissue growth**

(A–D) Expression pattern of *OBP1* (A,C) and *DOF5.8* (B,D) using whole-mount RNA *in situ* hybridization and transgenic plants expressing translational reporters.

(E) Aggravation of *mp*<sup>5319</sup> phenotype in multiple mutants with *obp1* and *dof5.8*.

(F–K) Transactivation of *OBP1* or *DOF5.8* in wild-type roots leads to additional cell division.

(L) Model showing early and delayed response genes and processes during floral primordia establishment.

Scale bars 20µm (A–D), 1.5mm (E) 50µm (F–H), 25µm (I–K).

tomato ortholog of DOF5.8/OBP1, SIDO9, acts downstream of auxin and controls inflorescence meristem and floral meristem differentiation via the regulation of cell division genes (Hu et al., 2022).

## DISCUSSION

Consistent with our data, the *DOF5.8* promoter is bound by MP in EMSA and ChIP experiments (Konishi et al., 2015). In addition, MP was found using DAP-seq to bind both *OBP1* and *DOF5.8* promoters in chromatin-free isolated genomic DNA (Data S7) (O'Malley et al., 2016). These published data indicate that these two DOFs are direct MP targets and under direct regulation by auxin signaling. Both genes are also directly activated by LFY in inflorescences, as demonstrated by ChIP and microarray experiments (Data S5, S6, and S7), and the *LFY* promoter is bound by the two DOFs in DAP-seq data, suggesting that they are potential transcriptional regulators of *LFY* (Data S7). Our analysis thus identifies *OBP1*, *DOF5.8*, and *LFY* as elements of a network under direct control by auxin and at the interface between growth regulation and flower identity specification (Figure 4L). Consistent with a recently proposed function for *LFY* in flower outgrowth (Chahtane et al., 2013; Yamaguchi et al., 2016), the regulation of both *OBP1* and *DOF5.8* by *LFY* and vice-versa creates a network revealed by our genome-wide analysis of auxin responses during flower initiation. This network could be essential in



setting the dynamics of the expression of the two *DOF* genes and the relative timing of growth and identity changes during early flower development, and further studies will be required to validate this hypothesis.

### Limitations of the study

Our study provides datasets of direct auxin target genes in the SAM. However, because of the technology used (Illumina short reads), alternatively spliced transcripts were not studied. In addition, genes regulated at a different level (translation, subcellular localization, etc ...) are not accounted for. Also, although some of the top target genes identified have been confirmed as expressed in floral organ primordia, alternative approaches such as RNA *in situ* hybridisation or transgenic reporter lines are needed to confirm their precise spatiotemporal expression pattern. Finally, functional redundancy remains the most likely explanation why we could not identify strong phenotypes in our double mutants as there are more than 30 additional *DOF* genes in the Arabidopsis genome.

### STAR★METHODS

Detailed methods are provided in the online version of this paper and include the following:

- KEY RESOURCES TABLE
- RESOURCE AVAILABILITY
  - Lead contact
  - Materials availability
  - Data and code availability
- EXPERIMENTAL MODEL AND SUBJECT DETAILS
  - Plant growth
- METHOD DETAILS
  - Constructs & plant transformation
  - RNA extraction and RNA-seq data analysis
  - Gene ontologies and heatmaps
  - Gene lists used and heatmaps
  - Whole mount *in situ* hybridisation
  - ARF5 dap-seq peaks
  - Microscopy
  - Phylogenetic tree
- QUANTIFICATION AND STATISTICAL ANALYSIS

### SUPPLEMENTAL INFORMATION

Supplemental information can be found online at <https://doi.org/10.1016/j.isci.2022.104683>.

### ACKNOWLEDGMENTS

We thank Carlos Galvan Ampudia for the DR5-3xVenus image (Figure 1A) and the members of the RDP SIGNAL team for fruitful discussions.

Funding: This work was supported by ANR-12-BSV6-0005 grant (Auxiflo) to T.V. and F.P. and Human Frontier Science Program organization (HFSP) Grant RPG0054-2013 to T.V.

### AUTHOR CONTRIBUTIONS

A.L., F.P., and T.V. designed the experiments. A.L., G.B., S.L., A.G., L.H., L.S.T., S.B., E.S., and I.S. performed experiments. A.S. and F.P. performed auxin responses elements density analyses. All authors were involved in data analysis. J.J. helped with RNA-seq analyses. A.L. and T.V. wrote the manuscript with inputs from all authors.

### DECLARATION OF INTERESTS

The authors declare that they have no competing interest.

Received: May 5, 2022  
Revised: June 13, 2022  
Accepted: June 23, 2022  
Published: July 15, 2022

## REFERENCES

- Armezzani, A., Abad, U., Ali, O., Robin, A.A., Vachez, L., Larrieu, A., Mellerowicz, E.J., Taconnat, L., Battu, V., Stanislas, T., et al. (2018). Transcriptional induction of cell wall remodelling genes is coupled to microtubule-driven growth isotropy at the shoot apex in Arabidopsis. *Development* 145, dev162255. <https://doi.org/10.1242/dev.162255>.
- Bell, E.M., Lin, W.c., Husbands, A.Y., Yu, L., Jaganatha, V., Jablonska, B., Mangeon, A., Neff, M.M., Girke, T., and Springer, P.S. (2012). Arabidopsis lateral organ boundaries negatively regulates brassinosteroid accumulation to limit growth in organ boundaries. *Proc. Natl. Acad. Sci. USA* 109, 21146–21151. <https://doi.org/10.1073/pnas.1210789109>.
- Bennett, S.R.M., Alvarez, J., Bossinger, G., and Smyth, D.R. (1995). Morphogenesis in pinoid mutants of Arabidopsis thaliana. *Plant J.* 8, 505–520. <https://doi.org/10.1046/j.1365-313X.1995.8040505.x>.
- Besnard, F., Refahi, Y., Morin, V., Marteaux, B., Brunoud, G., Chambrier, P., Rozier, F., Mirabet, V., Legrand, J., Lainé, S., et al. (2014). Cytokinin signalling inhibitory fields provide robustness to phyllotaxis. *Nature* 505, 417–421. <https://doi.org/10.1038/nature12791>.
- Brunoud, G., Wells, D.M., Oliva, M., Larrieu, A., Mirabet, V., Burrow, A.H., Beeckman, T., Kepinski, S., Traas, J., Bennett, M.J., and Vernoux, T. (2012). A novel sensor to map auxin response and distribution at high spatio-temporal resolution. *Nature* 482, 103–106. <https://doi.org/10.1038/nature10791>.
- Caggiano, M.P., Yu, X., Bhatia, N., Larsson, A., Ram, H., Ohno, C.K., Sappl, P., Meyerowitz, E.M., Jönsson, H., and Heisler, M.G. (2017). Cell type boundaries organize plant development. *Elife* 6, e27421. <https://doi.org/10.7554/eLife.27421>.
- Chahtane, H., Vachon, G., Le Masson, M., Thévenon, E., Périgon, S., Mihajlovic, N., Kalinina, A., Michard, R., Moyroud, E., Monniaux, M., et al. (2013). A variant of LEAFY reveals its capacity to stimulate meristem development by inducing RAX1. *Plant J. Cell Mol. Biol.* 74, 678–689. <https://doi.org/10.1111/tpj.12156>.
- Christensen, S.K., Dagenais, N., Chory, J., and Weigel, D. (2000). Regulation of auxin response by the protein kinase PINOID. *Cell* 100, 469–478. [https://doi.org/10.1016/s0092-8674\(00\)80682-0](https://doi.org/10.1016/s0092-8674(00)80682-0).
- De Rybel, B., Audenaert, D., Xuan, W., Overvoorde, P., Strader, L.C., Kepinski, S., Hoyer, R., Brisbois, R., Parizot, B., Vanneste, S., et al. (2012). A role for the root cap in root branching revealed by the non-auxin probe naxillin. *Nat. Chem. Biol.* 8, 798–805. <https://doi.org/10.1038/nchembio.1044>.
- Denay, G., Chahtane, H., Tichtinsky, G., and Parcy, F. (2017). A flower is born: an update on Arabidopsis floral meristem formation. *Curr. Opin. Plant Biol.* 35, 15–22. <https://doi.org/10.1016/j.cpb.2016.09.003>.
- Donner, T.J., Sherr, I., and Scarpella, E. (2009). Regulation of preprocambial cell state acquisition by auxin signaling in Arabidopsis leaves. *Development* 136, 3235–3246. <https://doi.org/10.1242/dev.037028>.
- Hagen, G., Martin, G., Li, Y., and Guilfoyle, T.J. (1991). Auxin-induced expression of the soybean GH3 promoter in transgenic tobacco plants. *Plant Mol. Biol.* 17, 567–579. <https://doi.org/10.1007/bf00040658>.
- Hamant, O., Nogué, F., Belles-Boix, E., Jublot, D., Grandjean, O., Traas, J., and Pautot, V. (2002). The KNAT2 homeodomain protein interacts with ethylene and cytokinin signaling. *Plant Physiol.* 130, 657–665. <https://doi.org/10.1104/pp.004564>.
- Heisler, M.G., Ohno, C., Das, P., Sieber, P., Reddy, G.V., Long, J.A., and Meyerowitz, E.M. (2005). Patterns of auxin transport and gene expression during primordium development revealed by live imaging of the Arabidopsis inflorescence meristem. *Curr. Biol.* 15, 1899–1911. <https://doi.org/10.1016/j.cub.2005.09.052>.
- Hu, G., Wang, K., Huang, B., Mila, I., Frasse, P., Maza, E., Djari, A., Hernould, M., Zouine, M., Li, Z., and Bouzayen, M. (2022). The auxin-responsive transcription factor SIDOF9 regulates inflorescence and flower development in tomato. *Nat. Plants* 8, 419–433. <https://doi.org/10.1038/s41477-022-01121-1>.
- Karimi, M., Depicker, A., and Hilson, P. (2007). Recombinational cloning with plant gateway vectors. *Plant Physiol.* 145, 1144–1154. <https://doi.org/10.1104/pp.107.106989>.
- Katoh, K., Rozewicki, J., and Yamada, K.D. (2019). MAFFT online service: multiple sequence alignment, interactive sequence choice and visualization. *Brief. Bioinform.* 20, 1160–1166. <https://doi.org/10.1093/bib/bbx108>.
- Kim, D., Perte, G., Trapnell, C., Pimentel, H., Kelley, R., and Salzberg, S.L. (2013). TopHat2: accurate alignment of transcriptomes in the presence of insertions, deletions and gene fusions. *Genome Biol.* 14, R36. <https://doi.org/10.1186/gb-2013-14-4-r36>.
- Konishi, M., Donner, T.J., Scarpella, E., and Yanagisawa, S. (2015). MONOPTEROS directly activates the auxin-inducible promoter of the Dof5.8 transcription factor gene in Arabidopsis thaliana leaf provascular cells. *J. Exp. Bot.* 66, 283–291. <https://doi.org/10.1093/jxb/eru418>.
- Konishi, M., and Yanagisawa, S. (2015). Transcriptional repression caused by Dof5.8 is involved in proper vein network formation in Arabidopsis thaliana leaves. *J. Plant Res.* 128, 643–652. <https://doi.org/10.1007/s10265-015-0712-0>.
- Landrein, B., Formosa-Jordan, P., Malivert, A., Schuster, C., Melnyk, C.W., Yang, W., Turnbull, C., Meyerowitz, E.M., Locke, J.C.W., and Jönsson, H. (2018). Nitrate modulates stem cell dynamics in Arabidopsis shoot meristems through cytokinins. *Proc. Natl. Acad. Sci. USA* 115, 1382–1387. <https://doi.org/10.1073/pnas.1718670115>.
- Larrieu, A., and Vernoux, T. (2015). Comparison of plant hormone signalling systems. *Essays Biochem.* 58, 165–181. <https://doi.org/10.1042/bse0580165>.
- Larrieu, A.P., French, A.P., Pridmore, T.P., Bennett, M.J., and Wells, D.M. (2014). Time-profiling fluorescent reporters in the Arabidopsis root. *Methods Mol. Biol.* 1056, 11–17. [https://doi.org/10.1007/978-1-62703-592-7\\_2](https://doi.org/10.1007/978-1-62703-592-7_2).
- Lee, S.B., and Suh, M.C. (2015). Cuticular wax biosynthesis is up-regulated by the MYB94 transcription factor in Arabidopsis. *Plant Cell Physiol.* 56, 48–60. <https://doi.org/10.1093/pcp/pcu142>.
- Liu, X., Huang, J., Wang, Y., Khanna, K., Xie, Z., Owen, H.A., and Zhao, D. (2010). The role of floral organs in carpels, an Arabidopsis loss-of-function mutation in MicroRNA160a, in organogenesis and the mechanism regulating its expression. *Plant J. Cell Mol. Biol.* 62, 416–428. <https://doi.org/10.1111/j.1365-313X.2010.04164.x>.
- Long, J.A., Moan, E.I., Medford, J.I., and Barton, M.K. (1996). A member of the KNOTTED class of homeodomain proteins encoded by the STM gene of Arabidopsis. *Nature* 379, 66–69. <https://doi.org/10.1038/379066a0>.
- Love, M.I., Huber, W., and Anders, S. (2014). Moderated estimation of fold change and dispersion for RNA-seq data with DESeq2. *Genome Biol.* 15, 550. <https://doi.org/10.1186/s13059-014-0550-8>.
- Mähönen, A.P., Bishopp, A., Higuchi, M., Nieminen, K.M., Kinoshita, K., Törmäkangas, K., Ikeda, Y., Oka, A., Kakimoto, T., and Helariutta, Y. (2006). Cytokinin signaling and its inhibitor AHP6 regulate cell fate during vascular development. *Science* 311, 94–98. <https://doi.org/10.1126/science.1118875>.
- Miyashima, S., Roszak, P., Seville, I., Toyokura, K., Blob, B., Heo, J.-O., Mellor, N., Help-Rinta-Rahko, H., Otero, S., Smet, W., et al. (2019). Mobile PEAR transcription factors integrate positional cues to prime cambial growth. *Nature* 565, 490–494. <https://doi.org/10.1038/s41586-018-0839-y>.
- Narsai, R., Gouil, Q., Secco, D., Srivastava, A., Karpievitch, Y.V., Liew, L.C., Lister, R., Lewsey, M.G., and Whelan, J. (2017). Extensive transcriptomic and epigenomic remodelling occurs during Arabidopsis thaliana germination. *Genome Biol.* 18, 172. <https://doi.org/10.1186/s13059-017-1302-3>.

- Okada, K., Ueda, J., Komaki, M.K., Bell, C.J., and Shimura, Y. (1991). Requirement of the auxin polar transport system in early stages of Arabidopsis floral bud formation. *Plant Cell* 3, 677–684. <https://doi.org/10.1105/tpc.3.7.677>.
- O'Malley, R., Huang, S.-S.C., Song, L., Lewsey, M.G., Bartlett, A., Nery, J.R., Galli, M., Gallavotti, A., and Ecker, J.R. (2016). Cistrome and epistrome features shape the regulatory DNA landscape. *Cell* 165, 1280–1292. <https://doi.org/10.1016/j.cell.2016.04.038>.
- Przemeck, G.K., Mattsson, J., Hardtke, C.S., Sung, Z.R., and Berleth, T. (1996). Studies on the role of the Arabidopsis gene MONOPTEROS in vascular development and plant cell axialization. *Planta* 200, 229–237. <https://doi.org/10.1007/BF00208313>.
- Reinhardt, D., Pesce, E.-R., Stieger, P., Mandel, T., Baltensperger, K., Bennett, M., Traas, J., Friml, J., and Kuhlemeier, C. (2003). Regulation of phyllotaxis by polar auxin transport. *Nature* 426, 255–260. <https://doi.org/10.1038/nature02081>.
- Rozier, F., Mirabet, V., Vernoux, T., and Das, P. (2014). Analysis of 3D gene expression patterns in plants using whole-mount RNA in situ hybridization. *Nat. Protoc.* 9, 2464–2475. <https://doi.org/10.1038/nprot.2014.162>.
- Sassi, M., Ali, O., Boudon, F., Cloarec, G., Abad, U., Cellier, C., Chen, X., Gilles, B., Milani, P., Friml, J., et al. (2014). An auxin-mediated shift toward growth isotropy promotes organ formation at the shoot meristem in Arabidopsis. *Curr. Biol.* 24, 2335–2342. <https://doi.org/10.1016/j.cub.2014.08.036>.
- Schmid, M., Davison, T.S., Henz, S.R., Pape, U.J., Demar, M., Vingron, M., Schölkopf, B., Weigel, D., and Lohmann, J.U. (2005). A gene expression map of Arabidopsis thaliana development. *Nat. Genet.* 37, 501–506. <https://doi.org/10.1038/ng1543>.
- Siligato, R., Wang, X., Yadav, S.R., Lehesranta, S., Ma, G., Ursache, R., Sevilem, I., Zhang, J., Gorte, M., Prasad, K., et al. (2016). MultiSite gateway-compatible cell type-specific gene-inducible system for plants. *Plant Physiol.* 170, 627–641. <https://doi.org/10.1104/pp.15.01246>.
- Skirycz, A., Radziejowski, A., Busch, W., Hannah, M.A., Czeszejko, J., Kwaśniewski, M., Zanor, M.-I., Lohmann, J.U., De Veylder, L., Witt, I., and Mueller-Roeber, B. (2008). The DOF transcription factor OBP1 is involved in cell cycle regulation in Arabidopsis thaliana. *Plant J. Cell Mol. Biol.* 56, 779–792. <https://doi.org/10.1111/j.1365-3113.2008.03641.x>.
- Staswick, P.E., Tiryaki, I., and Rowe, M.L. (2002). Jasmonate response locus JAR1 and several related Arabidopsis genes encode enzymes of the firefly luciferase superfamily that show activity on jasmonic, salicylic, and indole-3-acetic acids in an assay for adenylation. *Plant Cell* 14, 1405–1415. <https://doi.org/10.1105/tpc.000885>.
- Su, Z., Ma, X., Guo, H., Sukiran, N.L., Guo, B., Assmann, S.M., and Ma, H. (2013). Flower development under drought stress: morphological and transcriptomic analyses reveal acute responses and long-term acclimation in Arabidopsis. *Plant Cell* 25, 3785–3807. <https://doi.org/10.1105/tpc.113.115428>.
- Thomas, C.L., Schmidt, D., Bayer, E.M., Drees, R., and Maule, A.J. (2009). Arabidopsis plant homeodomain finger proteins operate downstream of auxin accumulation in specifying the vasculature and primary root meristem. *Plant J. Cell Mol. Biol.* 59, 426–436. <https://doi.org/10.1111/j.1365-3113.2009.03874.x>.
- Torti, S., Fornara, F., Vincent, C., Andrés, F., Nordström, K., Göbel, U., Knoll, D., Schoof, H., and Coupland, G. (2012). Analysis of the Arabidopsis shoot meristem transcriptome during floral transition identifies distinct regulatory patterns and a leucine-rich repeat protein that promotes flowering. *Plant Cell* 24, 444–462. <https://doi.org/10.1105/tpc.111.092791>.
- Verkest, A., Manes, C.L.d.O., Vercruyse, S., Maes, S., Van Der Schueren, E., Beeckman, T., Genschik, P., Kuiper, M., Inzé, D., and De Veylder, L. (2005). The cyclin-dependent kinase inhibitor KRP2 controls the onset of the endoreduplication cycle during Arabidopsis leaf development through inhibition of mitotic CDKA1 kinase complexes. *Plant Cell* 17, 1723–1736. <https://doi.org/10.1105/tpc.105.032383>.
- Vernoux, T., Brunoud, G., Farcot, E., Morin, V., Van den Daele, H., Legrand, J., Oliva, M., Das, P., Larrieu, A., Wells, D., et al. (2011). The auxin signalling network translates dynamic input into robust patterning at the shoot apex. *Mol. Syst. Biol.* 7, 508. <https://doi.org/10.1038/msb.2011.39>.
- Vernoux, T., Kronenberger, J., Grandjean, O., Laufs, P., and Traas, J. (2000). PIN-FORMED 1 regulates cell fate at the periphery of the shoot apical meristem. *Development* 127, 5157–5165. <https://doi.org/10.1242/dev.127.23.5157>.
- Weijers, D., Schlereth, A., Ehrismann, J.S., Schwank, G., Kientz, M., and Jürgens, G. (2006). Auxin triggers transient local signaling for cell specification in Arabidopsis embryogenesis. *Dev. Cell* 10, 265–270. <https://doi.org/10.1016/j.devcel.2005.12.001>.
- Winter, C.M., Austin, R.S., Blanvillain-Baufumé, S., Reback, M.A., Monniaux, M., Wu, M.-F., Sang, Y., Yamaguchi, A., Yamaguchi, N., Parker, J.E., et al. (2011). LEAFY target genes reveal floral regulatory logic, cis motifs, and a link to biotic stimulus response. *Dev. Cell* 20, 430–443. <https://doi.org/10.1016/j.devcel.2011.03.019>.
- Winter, C.M., Yamaguchi, N., Wu, M.-F., and Wagner, D. (2015). Transcriptional programs regulated by both LEAFY and APETALA1 at the time of flower formation. *Physiol. Plant.* 155, 55–73. <https://doi.org/10.1111/pp1.12357>.
- Wu, M.-F., Yamaguchi, N., Xiao, J., Bargmann, B., Estelle, M., Sang, Y., and Wagner, D. (2015). Auxin-regulated chromatin switch directs acquisition of flower primordium founder fate. *Elife* 4, e09269. <https://doi.org/10.7554/eLife.09269>.
- Xing, S., Rosso, M.G., and Zachgo, S. (2005). ROXY1, a member of the plant glutaredoxin family, is required for petal development in Arabidopsis thaliana. *Development* 132, 1555–1565. <https://doi.org/10.1242/dev.01725>.
- Yamaguchi, N., Jeong, C.W., Nole-Wilson, S., Krizek, B.A., and Wagner, D. (2016). AINTEGUMENTA and AINTEGUMENTA-LIKE6/PLETHORA3 induce LEAFY expression in response to auxin to promote the onset of flower formation in Arabidopsis. *Plant Physiol.* 170, 283–293. <https://doi.org/10.1104/pp.15.00969>.
- Yamaguchi, N., Wu, M.-F., Winter, C.M., Berns, M.C., Nole-Wilson, S., Yamaguchi, A., Coupland, G., Krizek, B.A., and Wagner, D. (2013). A molecular framework for auxin-mediated initiation of flower primordia. *Dev. Cell* 24, 271–282. <https://doi.org/10.1016/j.devcel.2012.12.017>.
- Yanagisawa, S. (2002). The Dof family of plant transcription factors. *Trends Plant Sci.* 7, 555–560. [https://doi.org/10.1016/s1360-1385\(02\)02362-2](https://doi.org/10.1016/s1360-1385(02)02362-2).
- Yang, D.-L., Yao, J., Mei, C.-S., Tong, X.-H., Zeng, L.-J., Li, Q., Xiao, L.-T., Sun, T.p., Li, J., Deng, X.-W., et al. (2012). Plant hormone jasmonate prioritizes defense over growth by interfering with gibberellin signaling cascade. *Proc. Natl. Acad. Sci. USA* 109, E1192–E1200. <https://doi.org/10.1073/pnas.1201616109>.
- Zhu, A., Ibrahim, J.G., and Love, M.I. (2018). Heavy-tailed prior distributions for sequence count data: removing the noise and preserving large differences. *Bioinformatics* 35, 2084–2092. <https://doi.org/10.1101/303255>.

STAR★METHODS

KEY RESOURCES TABLE

REAGENT or RESOURCE	SOURCE	IDENTIFIER
Chemicals, peptides, and recombinant proteins		
Sodium carbonate	Fluka	cat. no. 71350
Sodium acetate	Euromedex	cat. no. EU0310
Sodium hydrogen carbonate	Merck	cat. no. 6329
GoTaq reaction buffer, 5×	Promega	cat. no. M792A
Proteinase K	Invitrogen	cat. no. 25530.015)
Polyvinylpyrrolidone average molecular weight 40,000	Sigma-Aldrich	cat. no. PVP40-100g
Tween 20	Sigma-Aldrich	cat. no. P2287
Ficoll 400	Sigma-Aldrich	cat. no. F2637
Agarose	Euromedex	cat. no. DNA grade LE-8200.B
GoTaq DNA Polymerase	Promega	cat. no. M784A
Tris-HC (1 M, pH 8 and pH 9.5)	Euromedex	cat. no. 200923.A
Glacial acetic acid	VWR	cat. no. 20104.298)
DIG RNA labeling mix, 10× containing 10 mM ATP, 10 mM CTP, 10 mM GTP, 6.5 mM UTP and 3.5 mM DIG-11-UTP	Roche	cat. no. 11 277 073
Anti-digoxigenin-AP Fab fragments	Roche	cat. no. 11 093 274 910; RRID:AB_514500
4-Nitro blue tetrazolium (NBT) chloride solution	Roche	cat. no. 11 383 213 001
5-Bromo-4-chloro-3-indolyl-phosphate, 4-toluidine salt (BCIP) solution	Roche	cat. no. 11 383 221 001
BSA	Sigma-Aldrich	cat. no. A8022
Pectolyase Y23	Duchefa	cat. no. P9004.0001
Pectinase from <i>Aspergillus</i>	Serva	cat. no. 31660
Macerozyme R10	Duchefa	cat. no. M8002.0005
Cellulase RS	Duchefa	cat. no. C8003.0005
Histoclear II	VWR	cat. no. NADIHS-200-1GAL
Dulbecco's PBS, 10×	Scientific PAA	cat. no. H15-011
Methanol	VWR	cat. no. 1.06009.1000
Absolute ethanol	Elvetec	cat. no. 200093)
Formaldehyde (36% solution stabilized in 9% methanol)	VWR	cat. no. 20909.290
Hydrogen peroxide (H <sub>2</sub> O <sub>2</sub> ), 30% solution	Sigma-Aldrich	cat. no. 21.676.3
tRNA from baker's yeast	Roche	cat. no. 10 109 495
Salmon sperm DNA	Qbiogen	cat. no. SADN005
Trisodium citrate dihydrate	VWR	cat. no. 11A190004
Sodium chloride	Euromedex	cat. no. 1112.A
Magnesium chloride hexahydrate	Calbiochem	cat. no. 442611
Formamide	VWR	cat. no. 24311.291
EDTA	Euromedex	EU0007-C
DNase I	Ambion	AM1907
Glycogen from <i>Mytilus edulis</i>	Sigma-Aldrich	G1767
RNase inhibitor	Bioblock	EO0381
dNTPS	Qiagen	cat. no. 10881767001
T7 RNA Polymerase	Roche	cat. no. 10881767001

(Continued on next page)

**Continued**

REAGENT or RESOURCE	SOURCE	IDENTIFIER
Sodium hypochlorite solution	Merck	1056142500, CAS: 7681-52-9
Triton	Merck	X100, CAS: 9036-19-5
Dexamethasone	Merck	D4902, CAS: 50-02-2
$\beta$ -Estradiol	Merck	E2758, CAS: 50-28-2
NAA (1-Naphthaleneacetic acid)	Merck	35745, CAS: 86-87-3
NPA (N-1-Naphthylphthalamidic acid)	Merck	PS343, CAS: 132-66-1
Agarose	Sigma-Aldrich	A-2790, CAS: 9012-36-6
Plant agar	Meridis	P 1001-1, CAS: 9002-18-0
MS basal salt mixture, powder	Sigma-Aldrich	M5524
Arabidopsis medium	Duchefa	N/A; custom order with composition according to Hamant et al. (2002)

**Experimental models: Organisms/strains**

Columbia 0 accession (Col-0)	NASC	N1093
<i>mpS319</i> (Col-0)	Donner et al. (2009)	SALK_021319
<i>pin1-7</i> (Col-0)	Thomas et al. (2009)	SALK_047613
<i>pid-9</i> (Col-0)	Christensen et al. (2000)	N/A
<i>obp1</i> (Col-0)	Narsai et al. (2017)	SALK_049540
<i>dof5.8-2</i> (Col-0)	Konishi et al. (2015)	SALK_02270835
<i>dof58-3</i> (No-0)	This study	pst03057
<i>pDR5::3xVenus</i>	Vernoux et al. (2011)	N/A
<i>pAHP6::erGFP</i>	Mähönen et al. (2006)	N/A
<i>pSTM::YFP-H4</i>	Verkest et al. (2005)	N/A
<i>pRPS5A::GR-bdl</i>	Weijers et al. (2006)	N/A
<i>pCRE1[XVE]::OBP1/pSAPL::GFP-GUS</i>	This study	N/A
<i>pCRE1[XVE]::DOF5.8/pSAPL::GFP-GUS</i>	This study	N/A
<i>pRPS5A::OBP1-GFP</i>	This study	N/A
<i>pRPS5A::DOF5.8-GFP</i>	This study	N/A
<i>pOBP1::OBP1-mCherry</i>	This study	N/A
<i>pDOF5.8::DOF5.8-mCherry</i>	This study	N/A

**Software and algorithms**

Fiji	<a href="https://imagej.nih.gov/ij/">https://imagej.nih.gov/ij/</a>	1.51a
Zeiss LSM	<a href="https://www.embl.de/eamnet/html/body_image_browser.html">https://www.embl.de/eamnet/html/body_image_browser.html</a>	Zeiss
FastqQC	<a href="https://www.bioinformatics.babraham.ac.uk/projects/fastqc/">https://www.bioinformatics.babraham.ac.uk/projects/fastqc/</a>	0.11.3
Tophat2	Kim et al. (2013)	v2.0.14
htseq-count	<a href="https://htseq.readthedocs.io/en/release_0.11.1/count.html">https://htseq.readthedocs.io/en/release_0.11.1/count.html</a>	v0.9.1
DESeq2	Love et al. (2014)	v. 1.18.1
R	<a href="https://cran.r-project.org/">https://cran.r-project.org/</a>	3.3.1
Pheatmap	<a href="https://www.rdocumentation.org/packages/pheatmap/versions/1.0.12/topics/pheatmap">https://www.rdocumentation.org/packages/pheatmap/versions/1.0.12/topics/pheatmap</a>	1.0.12

**Deposited data**

Project (all datasets grouped in a single Project)	SuperSeries	GEO: GSE205299
--	-------------	----------------

## RESOURCE AVAILABILITY

### Lead contact

Further information and requests for resources and reagents should be directed to and will be fulfilled by the lead contact, Teva Vernoux ([teva.vernoux@ens-lyon.fr](mailto:teva.vernoux@ens-lyon.fr)).

### Materials availability

Plasmids generated in this study are available upon request.

### Data and code availability

RNA-seq data have been deposited at GEO and are publicly available as of the date of publication. Accession number is GSE205299. Microscopy data reported in this paper will be shared by the [lead contact](#) upon request.

This paper does not report original code.

Any additional information required to reanalyze the data reported in this paper is available from the [lead contact](#) upon request.

## EXPERIMENTAL MODEL AND SUBJECT DETAILS

All mutants used in this study are in Col-0 accession (except where indicated) and the alleles were: *mp*<sup>S319</sup> (T-DNA, SALK\_021319 (Donner et al., 2009)), *pin1-7* (T-DNA, SALK\_047613 (Thomas et al., 2009)), *pid-9* (T-DNA and small deletion (Christensen et al., 2000)), *obp1* (T-DNA, SALK\_049540 (Narsai et al., 2017)), *dof5.8-2* (T-DNA, SALK\_022708 (Konishi et al., 2015)), *dof58-3* (T-DNA, pst03057, No-0 accession)]. The following reporters and inducible lines were described previously: pDR5:3xVenus (Vernoux et al., 2011), pAHP6:erGFP (Mähönen et al., 2006), pSTM:YFP-H4 (Verkest et al., 2005), pRPS5A:GR-*bdl* (Weijers et al., 2006). The following reporters and overexpression lines are described in this study: pCRE1[XVE]:OBP1/pSAPL:GFP-GUS, pCRE1[XVE]:DOF5.8/pSAPL:GFP-GUS, pRPS5A:OBP1-GFP, pRPS5A:DOF5.8-GFP, pOBP1:OBP1-GFP and pDOF5.8:DOF5.8-GFP. Col-0 is the wild-type accession used for all experiments. Primers used for genotyping are indicated in [Table S2](#).

### Plant growth

All genotypes (except *mp*<sup>S319</sup>) were germinated on soil for RNA-seq (mutants and dex-inducible line), phenotyping, confocal microscopy and *in situ* hybridisation experiments. The plants were initially grown in short days (8h light, 20°C; 16h darkness, 20°C) for 3 weeks before being transferred to long days for an additional 3 weeks (16h light, 20°C; 8h darkness, 20°C) to synchronise flowering. Whenever meristems were dissected (for RNA-seq, phenotyping, confocal microscopy and *in situ*), plants had bolted few days before and stems were 2–5 cm high. Because *mp*<sup>S319</sup> homozygous mutants rarely develop a primary root they often fail to grow beyond the seedling stage. To improve recovery of homozygous mutants, sterilised seeds from a heterozygous parent were germinated on solid ½ Murashige and Skoog (MS, Sigma) salts (2.15 g/L, pH 5.7), 1% agar plates containing auxin (1-Naphthaleneacetic acid, NAA at 0.1 μM) and grown for 10 days in short days (8h light, 20°C; 16h darkness, 20°C). Plants with distinctive *mp* phenotypes (fused cotyledons) but with a visible and growing primary or adventitious roots were transferred on soil and grown for another 2 weeks before being transferred to long days for 3 weeks.

Seeds to generate NPA pins (RNA-seq and confocal microscopy) were surface-sterilised and germinated on solid Arabidopsis medium (modified MS, see (Hamant et al., 2002) for details) complemented with N-1-Naphthylphthalamic Acid (NPA, 10 μM) and grown for 2 weeks in long days (16 h light, 20°C; 8 h darkness, 20°C). NPA pins used for all experiments did not have any bumps visible on their flank and had a maximum height of 2 cm.

Seeds for *in vitro* cultures were sterilised in 20% bleach, 0.1% Triton for 20 min and rinsed three times with sterile water. Seeds for NPA pins were sown using top-agar to ensure they are evenly spaced, a key parameter to obtain good proportions (~10%) of pins with no visible morphological changes. After the third rinse, water was removed and molten Arabidopsis medium containing 10 μM NPA was added to the sterile seeds. Seeds were resuspended in the medium and immediately poured onto round petri dishes already containing 25 mL of solid Arabidopsis medium (with 10 μM NPA) to a density of around 100 seeds/plate. All seeds were vernalised on plates for 2 days before growing in growth rooms (see conditions above).

Seeds for *OBP1* and *DOF5.8* overexpression under oestradiol inducible pCRE1[XVE] promoter were sterilized with bleach containing 0.1% tween for 5 min and rinsed six times with sterile water. Seeds were vernalized for 3 days, sown on solid ½ MS medium and grown for 4 days in long day conditions (16 h light, 22°C; 8 h darkness, 22°C). Induction was performed by transferring 4 days old seedlings to medium with 5 μM 17β-oestradiol (Sigma). All transgenic lines generated in this study were selected based on a single locus insertion (segregation 3/1 of basta resistance at the T2 generation) and analyzed as homozygous at the T3 generation.

## METHOD DETAILS

### Constructs & plant transformation

*OBP1* and *DOF5.8* promoters and coding sequence were amplified from Col-0 DNA (they are both intronless) and cloned using Gateway BP (Invitrogen, promoters) or TOPO cloning (Invitrogen, coding sequences) following manufacturer's recommendations into pDONRP4-P1R (promoters) and pDONR221 (coding sequences). Overexpression (RPS5A promoter, DOF gene and GFP as C terminal fusion) and translational fusion (DOF promoter, DOF gene and mCherry as C terminal fusions) constructs were assembled using three-fragment Multi-Site Gateway cloning (Invitrogen) into the binary vector pB7m34GW (Karimi et al., 2007), transformed into Col-0 or *mp<sup>5319</sup>* and transgenic plants selected on Basta (10 mg/mL). For ectopic expression of *OBP1* and *DOF5.8* in the root, their coding sequences were assembled with stele-specific estradiol-inducible promoter (pCRE1[XVE]) into pHm43GW using Multi-Site Gateway cloning (Siligato et al., 2016), transformed into pSAPL:GFP-GUS (Miyashima et al., 2019) marker line and transgenic plants selected on hygromycin. Primers used for cloning are indicated in Table S2.

### RNA extraction and RNA-seq data analysis

#### RNA for mutants

Five Col-0 (wild-type control) primary inflorescences per biological replicate were dissected up to P6 (dissection time +/- 2 min) and a section of +/- 500 μm from the tip of the meristem cut and directly frozen in liquid N<sub>2</sub>. Five *pin* inflorescences per biological replicate were mechanically stimulated for 2 min to simulate dissection and a section of +/- 500 μm from the tip of the meristem cut and directly frozen in liquid N<sub>2</sub>. Care was made to harvest only healthy Col-0 and *pin* mutants with no morphological changes at the apex). To reduce any effects due to the circadian clock, biological replicates were harvested alternatively in the following order (Col-0 R1, *pin1* R1, *pid* R1, *mp* R1, Col-0 R2, etc ... up to R4) (total harvesting time ~2 h 30 min, 4 biological replicates each genotype). *pin1-7* and Col-0 control already described in Armezzani et al. (2018)).

#### RNA for dex-inducible

50 μL of a solution containing dexamethasone (dex) (Sigma, 50 μM (dissolved in DMSO)) or not (mock control, DMSO only) and Silwet L-77 (Lehle seeds, 0.01% final concentration) was placed on the top of a Col-0 (wild-type control) or pRPS5A:GR-*bdI* (Weijers et al., 2006) primary inflorescence. Silwet was used to ensure treatments reached the meristem. After 2 h of treatments, five mock and dex treated primary inflorescences per biological replicate were dissected up to P6 (dissection time +/- 2 min), and a section of +/- 500 μm from the tip of the meristem cut and directly frozen in liquid N<sub>2</sub> per biological replicate. To ensure each sample was treated for 2 h exactly, inflorescences were treated every 4 min to accommodate for dissection time. To reduce the effects of the circadian clock, biological replicates were harvested alternatively (Col-0 Mock R1, Col-0 Dex R1, GR-*bdI* Mock R1, GR-*bdI* Dex R1, Col-0 Mock R2, etc ... up to R4) (total harvest time ~2 h 40 min).

#### RNA for auxin treated NPA pins

A section of +/- 500 μm from the tip of 20 NPA pins per biological replicate with no visible bumps on their flanks were harvested and kept in 2 mL Eppendorf tubes containing 500 μL of liquid Arabidopsis medium with NPA at 10 μM. Once all samples were harvested, an equal volume of liquid Arabidopsis medium containing auxin (Sigma, NAA at 2 μM (1 μM final)) or not (mock control) and NPA (Sigma, 10 μM) was added. Treatments were performed for 30 min or 120 min after which all liquid medium was removed, and the samples directly frozen in liquid N<sub>2</sub>. To reduce the effects of the circadian clock, the treatments were started in such a way that all were harvested at the same time. The following samples were generated: Auxin 30 min R1, Mock 30 min R1, Auxin 120 min R1, Mock 120 min R1, Auxin 30 min R2, etc ..., up to R4.

All RNA extractions were performed using the Arcturus Pico Pure (Thermo Fischer) RNA extraction kit following manufacturer's recommendations. RNA quality was assessed with a Bioanalyser and only samples with a RIN >6 were used. Before sequencing, an aliquot of RNA (500 ng) from selected samples was used for cDNA synthesis using Superscript Reverse Transcriptase II and the expression of few targets genes (*AHP6*, *PIN1*, *MP*, *PID*) as well as a control gene (AT1G04850) tested using qPCR. Four biological replicates were initially generated for all samples and three were sequenced (those with highest RINs).

All the sequencing reactions were performed at the "Plateforme Transcriptome" located in Unité de Recherche en Génomique Végétale (URGV) at the Université d'Evry Val d'Essonne (now Institute of Plant Sciences Paris-Saclay (IPS2), Université Paris-Sud, Université d'Evry, Université Paris-Saclay). Libraries were prepared using the Agilent RNA6000 Nano kit and sequenced on a HiSeq2000 (Paired End 2 × 100b). Fastq files of the reads (with adaptors, reads with quality below 20 and reads mapping to the ribosomes removed) were downloaded from the sequencing lab server. Fastq files were analyzed with FastQC (v 0.11.3, no particular options), reads mapped to the Arabidopsis genome (TAIR10) using Tophat2 (v2.0.14 (Kim et al., 2013), options: -p8 -read-realign-edit-dist 0 -min-anchor-length 5 -min-intron-length 9 -max-intron-length 15000 -max-multihits 50 -no-coverage-search -microexon-search -min-segment-intron 8 -max-segment-intron 50000 -b2-very-sensitive -prefilter-multihits), and reads that mapped to exons counted using htseq-count (v0.9.1, option: htseq-count -f bam -r pos -m intersection-nonempty -s reverse). Number of reads.

Count reads matrices were analyzed using DESeq2 (v. 1.18.1 (Love et al., 2014)) with default options. The log<sub>2</sub> fold changes were shrunk using the lfcShrink function and the "apeglm" method (Zhu et al., 2018). The following comparisons were generated:

Mutants analyses: *pin1-7* vs Col-0, *pid-9* vs Col-0, *mps319* vs Col-0. All the values are in Data S1. Gene with incoherent fold changes (i.e. induced in one mutant but repressed in another) were tagged as "Incoherent FC" (n = 648/15829, 4%). *pin1-7* and Col-0 control already described in Armezzani et al. (2018)).

Auxin analyses: Col Dex vs Col Mock, GR-*bdl* Dex vs GR-*bdl* Mock, Auxin 30 Minutes vs Mock 30 Minutes, Auxin 120 Minutes vs Mock 120 Minutes. There were no DEGs in the Col Dex vs Col Mock comparison. This dataset was therefore not used in subsequent analyses.

Genes tagged as differentially expressed have an FDR <0.1 (default in DESeq2). Overlaps were computed in R using the package VennDiagram.

The auxin response transcriptome in roots was analyzed using GEO2R (GSE42896 [Auxin 2hrs: GSM1503030, GSM1053031, GSM1053032; Mock: GSM1053036, GSM1053037, GSM1053038]) with default options (except for "Category of Plat-form annotation to display on results" where "Submitter supplied" was used instead of "NCBI supplied").

### Gene ontologies and heatmaps

Gene lists were generated using excel and analyzed using Panther (<http://www.pantherdb.org/>). All the details (database version, type and version of test used) are indicated in Datas S2, S4, and S6. Heatmaps to represent enriched ontologies were generated using pheatmap. Briefly, the log<sub>10</sub> of the FDR obtained with Panther for selected ontologies (indicated on the heatmaps) were calculated, imported and analyzed in R with pheatmap.

### Gene lists used and heatmaps

The root dataset (GSE42896 (De Rybel et al., 2012)) was used to compare the auxin response transcriptome in shoots and roots. The samples (GSM1053031, GSM1053032, GSM1053036, GSM1053037, GSM1053038) were analyzed using GEO2R (<https://www.ncbi.nlm.nih.gov/geo/geo2r/>) and the results exported to excel for analysis. The At GenExpress datasets GSE5629, GSE5630, GSE5631, GSE5632, GSE5633 (Schmid et al., 2005) were downloaded from GEO (<https://www.ncbi.nlm.nih.gov/geo/>). The average expression values for selected samples (GSM131685, GSM131688, GSM131691, GSM131694, GSM131697, GSM131700, GSM131703, GSM131706, GSM131643, GSM131649, GSM131652, GSM131655, GSM131658, GSM131661, GSM131576, GSM131579, GSM131582, GSM131585, GSM131588, GSM131591, GSM131594, GSM131597, GSM131600, GSM131603, GSM131606, GSM131609, GSM131612, GSM131636, GSM131555, GSM131558, GSM131495,



GSM131498, GSM131507, GSM131510, GSM131513, GSM131516, GSM131519, GSM131522, GSM131528, GSM131531, GSM131534, GSM131537, GSM131540, GSM131546) were calculated and  $\log_2$  transformed. These were then extracted for selected genes and used to generate the heatmap (Figure 3D). The LEAFY targets were selected based on (Winter et al., 2015).

### Whole mount *in situ* hybridisation

Whole mount *in situ* hybridisation was performed as described previously (Rozier et al., 2014). Briefly, full length cDNAs were amplified using a forward primer, starting at the ATG, and a reverse primers with the T7 RNA polymerase promoter. Amplified cDNAs were transcribed with the T7 RNA polymerase (Invitrogen) in presence of DIG-labelled NTP mix (Roche). DNA was removed by DNase (Ambion) treatments and purified RNA were fragmented to 150 bp average size. Probes were quantified and kept in 50% formamide at  $-20^\circ\text{C}$ . Wild-type inflorescences were swiftly dissected, leaving a few flower primordia (up to P10), fixed in formaldehyde, dehydrated and kept in 100% methanol. Samples were rehydrated and the cell wall partially digested before performing the hybridisation overnight at  $50^\circ\text{C}$ . Anti-DIG-AP Fab fragments (Roche) antibody was used to detect the probes with an NBT/BCIP staining.

### ARF5 dap-seq peaks

Genes were classified in different groups: induced/repressed by auxin after 30/120 min and induced/repressed by dex. We defined their respective promoters as a (-2000, 3000) base pairs region around the respective gene transcription start site. For each of the aforementioned groups, we investigated the density of ARF5 DAP-Seq peaks (reduced to a 1 bp regions at their center) in the promoters of their respective genes, treating separately the 5001 positions (Figures S3C–S3H). To check for a potential enrichment of ARF binding sites in the differentially expressed genes compared to the non-varying ones, we pooled all the genes either responsive to DEX or auxin treatment and counted how many of them had at least one ARF5 dap-seq peak overlapping with their promoter. We then proceed to do the same in the group of non-regulated genes, so that we could perform a hypergeometric test.

### Microscopy

Fluorescent lines were observed using an inverted LSM700 confocal microscope with a water-dipping 40x lens. Dissected inflorescence (up to P6, i.e. when the meristem is visible) or NPA pins were removed from the plant and transferred onto solid  $\frac{1}{2}$  MS in small round Petri dishes. Cell walls were stained with propidium iodide (10  $\mu\text{g}/\text{mL}$ ). Just before observation, dissected inflorescences were submerged with sterile distilled water and NPA pins submerged with liquid Arabidopsis medium containing 10  $\mu\text{M}$  NPA with or without auxin (NAA at 1  $\mu\text{M}$ ). Confocal images were analyzed using Fiji (<https://fiji.sc/>). Quantification of fluorescence was carried out as described previously (Larrieu et al., 2014). Inflorescences used for *in situ*s as well as dissected siliques were observed using a dissecting microscope. Roots were stained with propidium iodide (10  $\mu\text{g}/\text{mL}$ ) and observed using Leica TCS SP5 II HCS-A confocal microscope with a water-dipping 60x lens.

### Phylogenetic tree

The phylogenetic tree of Arabidopsis DOF proteins was drawn using conserved, ungapped, amino acid sites of all DOF proteins with MAFFT (<https://mafft.cbrc.jp/> (Katoh et al., 2019)).

### QUANTIFICATION AND STATISTICAL ANALYSIS

For all the experiments, detail of statistical tests used and error-bars on barplots are indicated in the figure legends.